Fabrication and validation of a multi-channel type microfluidic chip for electrokinetic streaming potential devices

Myung-Suk Chun,* Min Suk Shim and Nak Won Choi†

Received 10th October 2005, Accepted 12th December 2005
First published as an Advance Article on the web 6th January 2006
DOI: 10.1039/b514327f

To elaborate on the applicability of the electrokinetic micro power generation, we designed and fabricated the silicon-glass as well as the PDMS-glass microfluidic chips with the unique features of a multi-channel. Besides miniaturizing the device, the key advantage of our microfluidic chip utilization lies in the reduction in water flow rate. Both a distributor and a collector taking the tapered duct geometry are positioned aiming the uniform distribution of water flow into all individual channels of the chip, in which several hundreds of single microchannels are assembled in parallel. A proper methodology is developed accompanying the deep reactive ion etching as well as the anodic bonding, and optimum process conditions necessary for hard and soft micromachining are presented. It has been shown experimentally and theoretically that the silicon-based microchannel leads to increasing streaming potential and higher external current compared to those of the PDMS-based one. A proper comparison between experimental results and theoretical computations allows justification of the validity of our novel devices. It is useful to recognize that a material inducing a higher magnitude of zeta potential has an advantage for obtaining higher power density under the same external resistance.

Introduction

The streaming potential is the opposite electrokinetic phenomenon to electro-osmosis in that it uses motion to produce an electric field. Such electrokinetic behavior is basically present due to the electric double layer (EDL), which forms as a result of the distribution of electric charges near a charged surface.[1] Electrokinetic phenomena have been necessarily concerned in the design of diagnostic microdevices and micro-chips,[2] particle manipulation techniques,[3] and micro flow control in micro-electro mechanical system (MEMS) devices.[4,5]

According to the general theory of Helmholtz, the streaming potential occurs owing to the charge displacement in the EDL caused by an external force shifting the liquid phase tangentially against the solid. As illustrated in Fig. 1, the counter-ions in the diffusive part of the EDL are carried toward the downstream end for the applied pressure p and the accumulation of ions sets up an electric field. Then the electric convection current (namely, streaming current) I_S results in the pressure-driven flow direction of electrolyte solution, and the streaming potential ϕ generates across the two ends with a channel length corresponding to this streaming current. This flow-induced streaming potential acts to drive the counter-ions in the mobile part of the EDL to move in the direction opposite to the streaming current, which will generate the conduction current I_C in the Stern layer of the EDL.[6–9] Here, the charge and electric potential distributions are obtained by solving the Poisson–Boltzmann (P–B) equation. The overall result is a reduced flow rate in the direction of the pressure drop referred to as the electroviscous effect.[10,11]

The convective transport of hydrodynamically mobile ions can be detected by measuring the streaming potential between the two electrodes positioned up- and downstream in the liquid

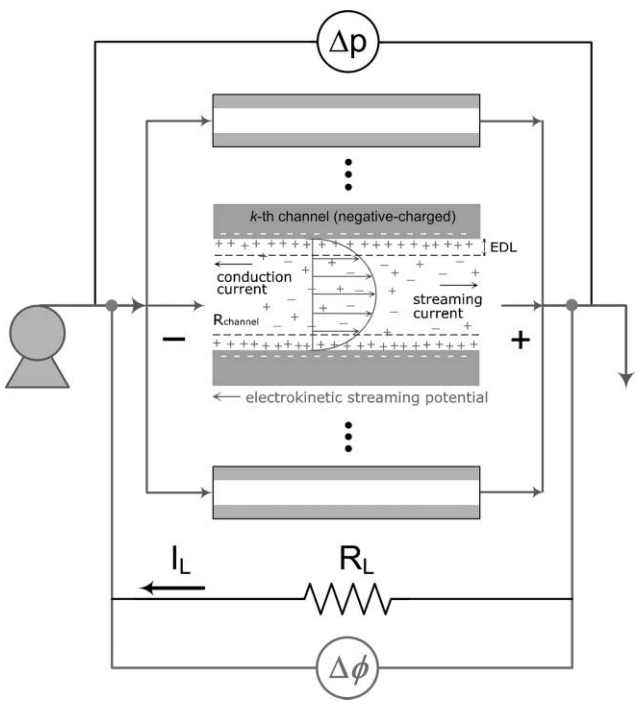

Fig. 1 Schematic diagram of the development of flow-induced streaming potential along a charged microchannel and the multi-channel array circuit with external resistance.

Complex Fluids Research Laboratory, Korea Institute of Science and Technology (KIST), PO Box 131, Cheongryang, Seoul 130-650, Republic of Korea. E-mail: mschun@kist.re.kr; Fax: +82-2-958-5205; Tel: +82-2-958-5363
† Present address: School of Chemical and Biomolecular Engineering, Cornell University, Ithaca, NY 14853, USA.

flow, when the internal resistance of the voltmeter used is sufficiently high. In Fig. 1, the external resistance R_L is applied in the multi-channel array circuit assembled with N channels in parallel. Then, the net current I equals $N(I_S + I_C) + I_L$, where I_L denotes the external current. It is taken to be zero at the steady state, *viz*. $I \equiv N(I_S + I_C) + I_L = 0$.

A recent paper by Yang *et al.*[12] revealed a new fact that the streaming potential is applicable to an electrokinetic micro battery consisting of an array of microchannels. They found a good agreement between the prediction and experimental results for pressure-driven flow in microporous glass filter with a nominal pore size of 10–16 μm. Their results suggest that the hydrostatic pressure of water can be converted into electrical work as a function of the properties of the electrolyte solution and channel wall. Subsequently, Olthuis *et al.*[13] also presented experimental results of the streaming potential and electric power with variations of external resistance by flowing the electrolyte solution through a microporous glass funnel with 1.0–1.6 μm pore sizes. They remarked on the need for a proper micromachined device such as a lab-on-a-chip for optimized energy transfer.

Very recently, Chun *et al.*[14] dealt with an in depth analysis of the microfluidics in a microchannel encompassing electrokinetic phenomena. They developed the Navier–Stokes (N–S) momentum equation for an incompressible ionic fluid by verifying the external body force and the relevant flow-induced electric field, from the theoretical analysis coupled with the full P–B equation. The basic principle of net current conservation was faithfully applied in the microchannel taking into account the Nernst–Planck equation. Considering the streaming potential in a multi-channel array circuit, they pointed out more useful microdevices such as a microfluidic chip with multi-channel type, instead of the glass filter.

With emerging MEMS technologies and micromachining techniques, the streaming potential will become an established process in the field of electrokinetic microfluidics. The adoption of a microfluidic chip for the electrokinetic streaming potential device allows us to access a more efficient system. The microfluidic chip makes the miniature device more compact, from which we can take advantage of reduced amounts of water required. Furthermore, a well-defined microchannel easily permits achieving more accurate control of the microflow.

It is the aim of this paper to investigate the fabrication of a high-density multi-channel type microfluidic chip for a streaming potential device as well as its performance test for applicability toward electrokinetic micro power generation. We have prepared two kinds of microfluidic chip: silicon-glass chip by dry etching and polydimethylsiloxane (PDMS)–glass chip by soft lithography. Silicon processing is practically associated with high quality and well-known standard technology.[15] For the uniform distribution of water flow into each of the individual channels, the microfluidic chip is designed to comprise a distributor and a collector, in which their unique features have tapered geometry subject to a constant variation rate. A pair of electrodes is positioned at the input as well as the output sides of the multi-channel by favorably inserting into the insertion space. To obtain the prototypes, we have fully considered optimum process parameters such as deep reactive ion etching (DRIE) conditions. Setting up the streaming potential system, both the streaming potential and corresponding electric current are measured for each of the chips, from which the electric power density is determined. Experimental results are compared with results from computations based on our previous theoretical work.

MEMS fabrications

Design of microfluidic chip with multi-channel mode

Once the fluid flows through each of the channels, which are accurately and regularly arranged, an electric potential difference occurs between both ends of an inlet and an outlet of the flow channel by the contribution of the streaming potential. In Fig. 2, the supplied fluid through the inflow port flows into individual channels by the distributor, and the eluting fluid gathered by the collector flows into the outflow port. Both the distributor and the collector take the tapered duct geometry aiming identical flow resistance for all individual channels, wherein cross-sectional areas change uniformly along the multi-channel span. If the distributor is designed in a parallel shape without tapering, the fluid flowing into the channel located at the side of the inflow port flows possibly out to the collector before the fluid enters the channel located at the opposite side. As a result, the ratio of streaming potential difference to pressure difference will necessarily decrease according to the well-known Helmholtz–Smoluchowski (H–S) formula,[9] which may result in an unstable electric energy. For this reason, the requirement of uniform flow distribution must be emphasized for multi-channel design.

When both the distance of the longer base and that of the shorter one in the tapered duct denote b_l and b_s respectively, the tapering rate of the distance r_t is defined as

$$r_t \equiv \frac{b_l - b_s}{L} = \frac{b_l - b_s}{NW + (N-1)S} \quad (1)$$

where L is the straight length of the duct that equals the span of the multi-channel with the number of microchannels N, W is the width of a single channel, and S is the inter-channel distance. In this study, base distances of b_l and b_s have fixed values of 800 μm and 300 μm, respectively. The multi-channel is formed to the same depth coincident with the distributor as well as the collector. The ratio of the channel depth to the inter-channel distance is usefully chosen to be less than 2 in order to endure against the applied pressure difference up to 3 bar.

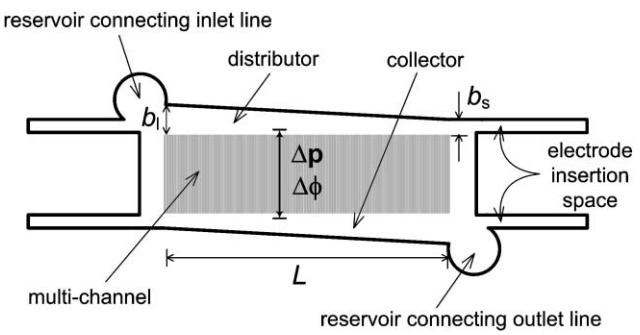

Fig. 2 A layout of photomask for fabricating a microfluidic chip with high-density multi-channel type.

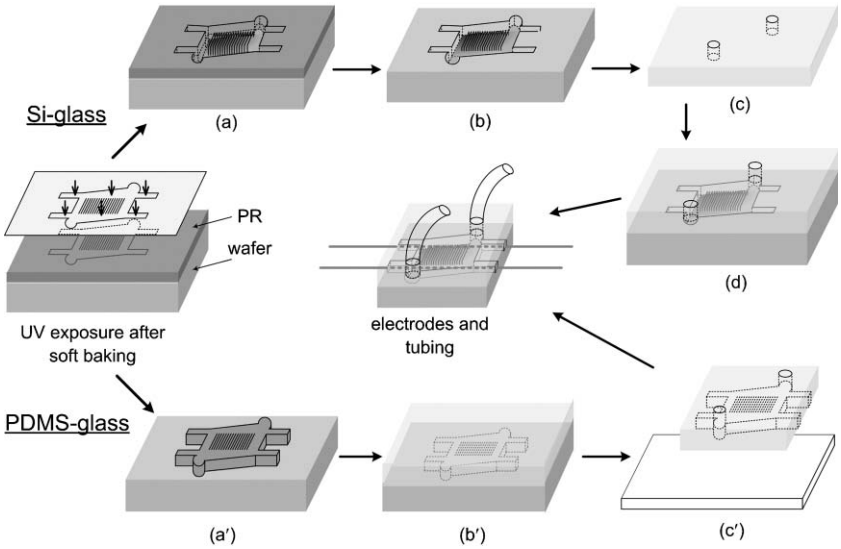

Fig. 3 Fabrication process for the multi-channel microfluidic chip. For silicon-glass, (a) positive PR developing, (b) dry etching and PR stripping, (c) glass cover drilling, and (d) anodic bonding. For PDMS-glass, (a′) negative PR developing, (b′) PDMS curing, and (c′) bonding PDMS replica with glass cover.

Electrodes are installed at both regions of the distributor and the collector, in which appropriate spaces exist for extending the electrodes to the external electric circuit. The space dimension is designed to be optimum to insert the electrode therein. The diameter of the inflow and the outflow ports is set to 1.6 mm so as to properly connect with the external flow tube of 1/16 inch outer diameter. Design was performed with a computer-aided program (AutoCAD® 2004, CA), and a high-resolution chromium mask supplied by the photomask manufacturer was prepared to minimize the surface roughness of the flow channel.

Microfluidic chip fabrications

Prior to the lithography process, the boron-doped silicon wafer (LG-Siltron Inc., P-100, Korea) was cleaned in boiling Piranha solution. In order to improve adherence of the photoresist (PR) onto the hydrophilic surface, the silicon wafer was spin-coated with a hexamethyldisilazane solution and baked.[16,17] The wafer was then coated with an AZ7220 positive PR (Clariant Corp., Switzerland) at 2500 rpm and baked at 100 °C. We carried out the spin coating once again with a soft baking process to get 4 μm thickness of the PR. In Fig. 3, the UV lithography was processed using a mask aligner (MA6, Karl Süss) with an intensity of 17 mW cm^{-2}. The PR was developed by immersing into the AZ400K developer dilute solution, and the hard baking was carried out at 140 °C for 10 min. The requirement was to form high-aspect-ratio channels with 100 μm depth onto the wafer to embed the electrodes of 100 μm diameter. As illustrated in Fig. 3(a), silicon DRIE (often called ''deep trench etching'') was performed by the Bosch process in the multiplex inductively coupled plasma system at 900 W with 13.56 MHz.[18,19] Both SF_6/O_2 etching and C_4F_8 passivating gases were respectively supplied with 130/13 and 110 sccm, underlying the switch for 45 min at 15 mTorr. After completing the DRIE, the PR was stripped using acetone (Fig. 3(b)).

Fig. 3(c) shows the holes to the inflow and outflow ports manufactured by drilling the Pyrex 7740 glass wafer with Nd:YAG laser. The thermal expansion of the glass wafer (*i.e.*, 2.9×10^{-6} K^{-1}) is similar to that of the silicon one (*i.e.*, 2.6×10^{-6} K^{-1}), that satisfactorily avoids a stress in the final structure.[20] The glass wafer with drilled via-holes was cleaned using the Piranha solution followed by deionized (DI) water. Whilst the thermal bonding is likely to bring channel deformations, the anodic bonding has the advantage of being a lower residual stress and requiring less stringent quality of substrate surface.[21–23] Sodium ions in the glass move towards the cathode of the applied voltage, and a space-charge region is developed from accumulations of the relatively immobile oxygen anions at the interface between silicon and glass. The high electric field results in an electrostatic force that brings an intimate contact.[24] Drifting the oxygen anions causes a development of the thin oxide layer and binding two substrates together as displayed in Fig. 3(d). Anodic bonding has been performed using a wafer bonder at 320 °C, 0.5 kV and 1.0 kg_f cm^{-2}. A pair of Ag/AgCl electrodes was inserted into both sides of the electrode insertion spaces of the chip, and polyethylethylketone (PEEK) tubes with 0.055 inch inner diameter were fixed at each port by means of epoxy glue.

We also prepared another chip using molded PDMS and glass coverslip by means of the soft lithography, as found in the relevant literature.[25,26] The SU8-50 negative PR was spin-coated on the silicon wafer to obtain the 100 μm height, which becomes the channel depth later. Soft baking was carried out and then the UV exposure was done with a power of 30 mW cm^{-2} and wavelength of 365 nm. Subsequently, a post exposure bake was performed so as to selectively cross-link the exposed portions. After removing the unexposed PR by the SU8 developer (MicroChem Co.), a master mold containing negatively-patterned PR was remained as depicted in Fig. 3(a′). In Fig. 3(b′), preliminary tubing was exactly placed on the corresponding inflow and outflow ports before the pouring a

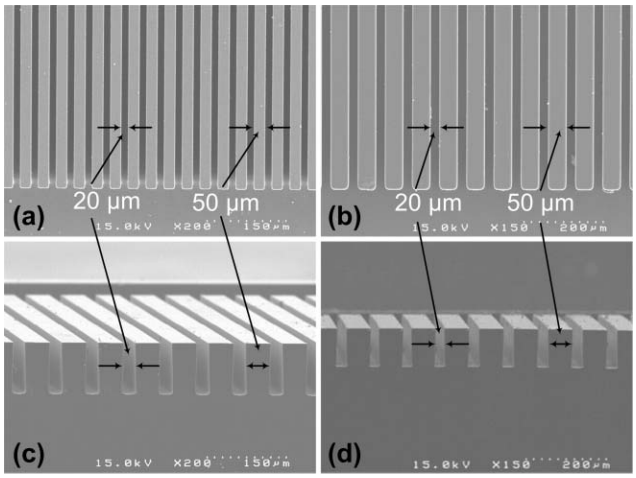

Fig. 4 SEM images of the multi-channel: (a) top view of the silicon-glass chip, (b) top view of the PDMS-glass chip, (c) cross-sectional view of the silicon-glass chip, and (d) cross-sectional view of the PDMS-glass chip.

10:1 mixture of PDMS (Sylgard 184, Dow Corning) pre-polymer and curing agent.[27] The cured PDMS replica was peeled from the master, and then we applied the RIE, where both the replica and the glass surfaces were sealed each other as shown in Fig. 3(c′). Likewise in the silicon-glass chip, a pair of the electrodes was inserted. Permanent PEEK tubes were installed at each port after removing the preliminary tubing.

Fig. 4 shows both the top and cross-sectional views of the multi-channel created on the silicon wafer as well as the PDMS replica. The cross section of the channel was quantified by a profilometer (Alpha Step 200, Tencor Instruments) prior to bonding the glass cover. It is faithfully found that individual channels are 100 μm deep, 20 μm wide at half-depth, and the inter-channel distance of 50 μm. While a higher anisotropy in the channel of the silicon wafer is achieved by employing the DRIE, the shape of the channel in the PDMS replica is somewhat trapezoidal. However, the underlying reason for producing this shape is different from isotropic etching.

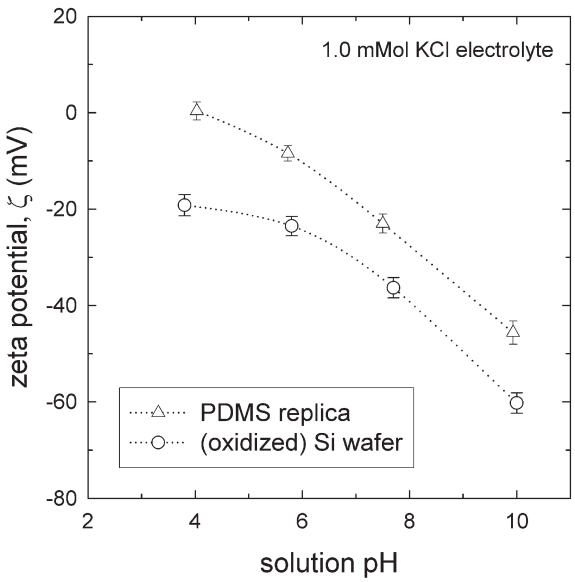

Fig. 5 The zeta potential characterization of microfluidic chip materials of silicon and PDMS surfaces.

Electrokinetic experiments

Surface characterization

To examine the charge property of channel surfaces regarding the silicon wafer and the PDMS replica, the zeta potential was measured with an electrophoretic light scattering spectrophotometer (ELS-8000, Otsuka Electronics, Osaka). The zeta potential quantified by experiments is hypothetically equivalent to the electric surface potential.[9,28] As shown in Fig. 5, both materials exhibit that the magnitude of the negative zeta potential increases with increasing pH of electrolyte solution. It is evident that the silicon surface is considered to be strongly charged as being due to its higher magnitude of negative zeta potential than that of the PDMS. Here, the silicon surface is covered with a thin film (*cf.*, in the range 1–2 nm) of SiO_2 due to native oxidation, resulting in a non-conducting nature.

Microflow system

Fig. 6(a) shows the prototype made by the step in Fig. 3. The microfluidic chip is fixed on a printed circuit board (PCB)

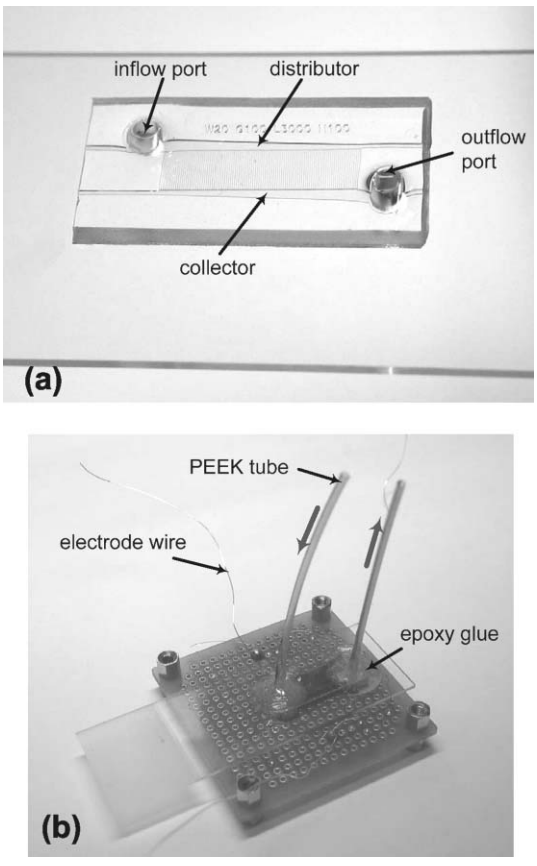

Fig. 6 (a) Close-up view of the multi-channel formed in the PDMS replica bonded with glass coverslip, and (b) microfluidic chip mounted on the PCB.

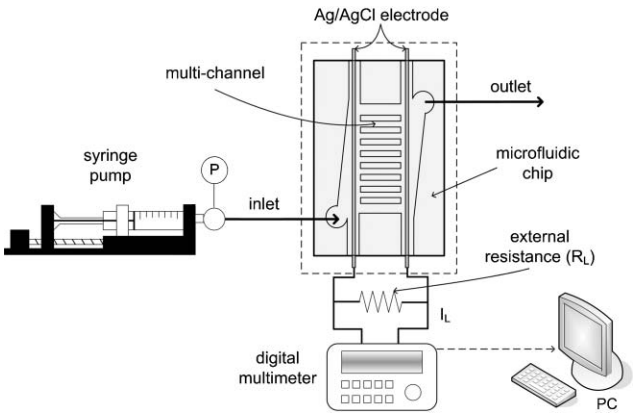

Fig. 7 Schematic of the experimental setup with electrokinetic streaming potential device.

frame as shown in Fig. 6(b), where the electrodes are connected to the external circuit to measure the streaming potential. The wire-type Ag/AgCl electrodes were prepared by anodic deposition of chloride on silver wire with a DC power supply (Consort E832, Belgium) at 0.4 mA cm^{-2} for 20 min.

The experimental setup is demonstrated in Fig. 7. The working fluid prepared with DI water (Elgastat Prima RO, UK) is carefully supplied into the inflow port of the microfluidic chip by a syringe pump (Cole-Parmer 74900 Series, IL). The ionic strength of working fluid was maintained as 2×10^{-3} mM KCl electrolyte for its thicker EDL, corresponding to 215 nm thickness. A high-precision pressure gauge with 0.1% FS accuracy (FD2000, Honeywell Sensotec, OH) was positioned to measure the pressure drop across the microchannel. The streaming potential difference between both ends of microchannels was detected using a digital multi-meter (HP34970A, Hewlett-Packard Co., CA) connected to a pair of Ag/AgCl electrodes. The potential readings were automatically stored in the computer for subsequent data processing. The pH of the working fluid was maintained as about 6.7.

Results and discussion

Multi-channel array without external resistance

Following the above procedure, we first measured the streaming potentials without external resistance generating from the silicon-glass and the PDMS-glass microchannels according to an increase of applied pressure difference. Each chip has the tapering rate as 0.036, estimated by eqn (1). The pressure difference was limited up to 1.8 bar in order to overcome the expansion occurring in the PDMS-glass microchannel. On the basis of the theory of H–S, one could expect the streaming potential ϕ to follow a linear relationship with pressure difference Δp as shown in Fig. 8. For silicon–glass microchannel, the increasing tendency in streaming potential is more considerable, and accordingly its value of streaming potential is higher than the PDMS–glass one. Regarding this fact, we point out that the magnitude of zeta potential of the silicon wafer at pH of 6.7 is *ca.* 1.7 times greater than that of the PDMS replica as presented in Fig. 5. This result is consistent with those in the literature,[12,14] where theoretical results

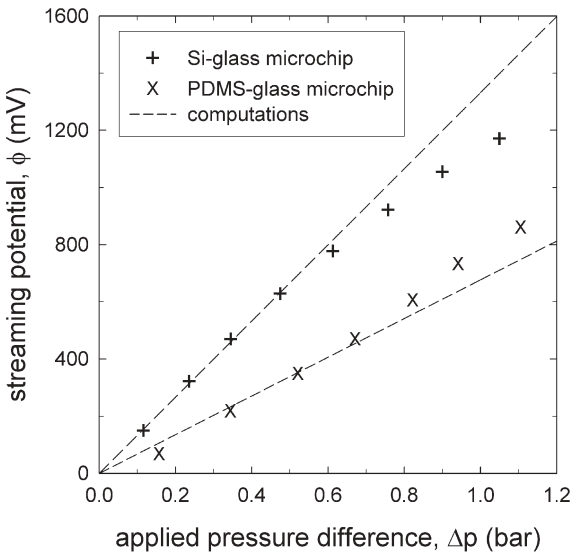

Fig. 8 The streaming potential *versus* pressure difference in silicon-glass and PDMS–glass microfluidic chips without external resistance. Each of the number of channels is 200.

provide that a higher magnitude of zeta potential in the channel wall results in a higher streaming potential.

In order to verify experimental results, we try to implement a computation of the streaming potential by the use of our previous theoretical model developed in the cylindrical channel,[14] with combining the correction of flow rate in rectangular channels. For a cross-sectional area A and the length l of the channel, the streaming current I_S defined as an integration of the product of the net charge density ρ_e and the axial velocity profile v_z takes the form

$$I_S \equiv \int_A \rho_e v_z \mathrm{d}A = f_{(1)} \frac{\Delta p}{l} + f_{(2)} \frac{\Delta \phi}{l} \tag{2}$$

where $f_{(1)}$ and $f_{(2)}$ denote the implicit coupled functions involving integrals. The Boltzmann distribution of the ionic concentration of type i, n_i ($=n_b \exp(-Z_i e\psi/kT)$) provides a local charge density at the electroneutral state, and the electric potential ψ is obtained from the numerical solution of the P-B equation. Then, $\rho_e = -2Zen_b \sinh(Ze\psi/kT)$, where Z is the valence of ions, e the elementary charge, kT the Boltzmann thermal energy, and the electrolyte ionic concentration in the bulk n_b ($1/m^3$) equals to the product of the Avogadro's number (1/mol) and bulk electrolyte concentration (mM). A formula for the v_z is established by analysis of the N–S equation including the body force term generated by an interaction between the ion charges of the EDL and the external electric field. Detailed descriptions have been provided in the previous paper.

The conduction current I_C is caused through the channel wall as well as the electrolyte solution, and then the Ohm's rule can be applied, yielding

$$I_C \equiv \frac{\Delta \phi}{R_T} \tag{3}$$

where the total resistance R_T along the channel consists of the surface resistance and the fluid resistance in parallel. The

principle of net current conservation without external resistance (*i.e.*, $I \equiv I_S + I_C = 0$) leads to the following expression

$$\Delta\phi = -\frac{f_{(1)}\Delta p}{\frac{l}{R_T} + f_{(2)}}. \quad (4)$$

On the basis of the fluid mechanics in laminar flow problem, it is possible to compare the flow rate in a rectangular channel to that in a cylindrical channel. If we take Q_C to be the volumetric flow rate from a circular capillary with the same cross-sectional area as a rectangular channel Q_R, we find $Q_R/Q_C = 0.369$ so that the correction of streaming potential can be provided. This approach is considered as a reasonable comparison without great deviation, even though it cannot be exact. In Fig. 8, the discrepancy between experiments and corresponding computations has been ascribed to this restriction. However, it is true that our experimental results have an approximate trend to agree with the computations.

Multi-channel array with external resistance

Once the external resistance R_L is applied in the multi-channel array assembled in parallel, the external current I_L passing this resistance can be measured. Fig. 9 shows that the external current of the silicon–glass chip is larger than that of the PDMS–glass one under identical channel dimensions as well as the same conditions. A higher surface potential possibly causes a higher charge density in EDL, and then more movable ions will induce a larger streaming current along the external current. Applying the current continuity principle (*i.e.*, $N(I_S + I_C) + I_L = 0$) again, the streaming potential in this multi-channel array circuit is expressed as

$$\Delta\phi_L = -\frac{f_{(1)}\Delta p}{\frac{l}{R_T} + \frac{l}{NR_L} + f_{(2)}} \quad (5)$$

from which one can compute the external current $I_L = \Delta\phi_L/R_L$ to verify experimental results. In view of Ohm's rule, the external current is in inverse proportion to the overall resistance consisting of the total channel resistance R_T/N and the external resistance R_L.[12] When the external resistance R_L is sufficiently small compared to the total channel resistance (*i.e.*, $R_T/N \gg R_L$), the external current can be written as

$$I_L = -\frac{Nf_{(1)}\Delta p}{l + NR_L f_{(2)}}. \quad (6)$$

In accordance with eqn (6), the external current is inversely proportional to the external resistance, as provided in Fig. 9. However, the external current changes very slightly with variations of the external resistance up to R_T/N.

The electric power density allows us to figure out the reliability of our novel microfluidic chip aiming for electrokinetic micro power generation. It can be estimated from the electric power divided by the overall volume of flow channels for the imposed external resistance, given as

$$P_D = \frac{\Delta\phi_L I_L}{N(HWl)}. \quad (7)$$

In Fig. 10, the power density increases with increasing either the magnitude of the zeta potential or external resistance R_L, identifying a reasonable agreement with the theoretical prediction.[14] It appears that the discrepancy between the two results on the Δp change is increased for the R_L of 1.0 kΩ. In the silicon–glass chip with an R_L of 1.0 kΩ, the power density has the highest value amongst our results. If the value of external resistance is further increased up to R_T/N, one can observe a higher order of magnitude for the power density as reported in the literature.[13] On the contrary, the power density is expected to have a decreasing behavior, when the external resistance becomes larger than R_T/N.

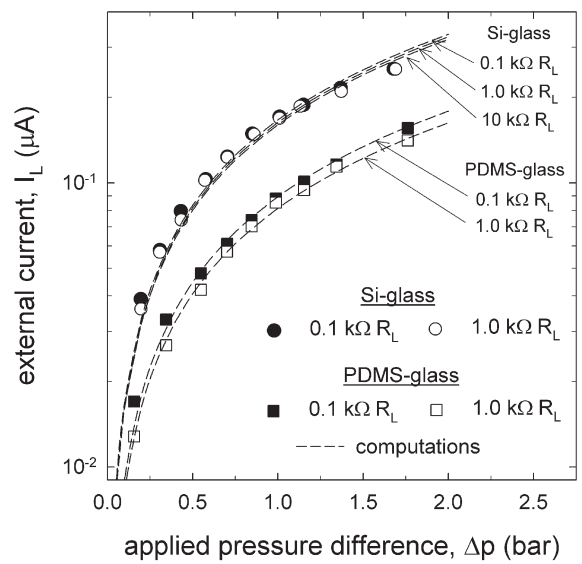

Fig. 9 The external electric current *versus* pressure difference in silicon–glass and PDMS–glass microfluidic chips with external resistances of 0.1 and 1.0 kΩ.

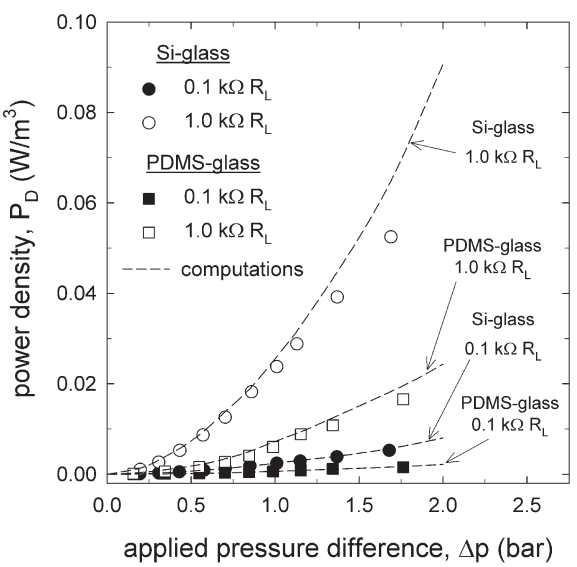

Fig. 10 The power density *versus* pressure difference in silicon–glass and PDMS–glass microfluidic chips with external resistances of 0.1 and 1.0 kΩ.

Conclusions

We have developed a high-density multi-channel type microfluidic chip capable of generating of electrokinetic streaming potential and external electric current realizing the H–S principle. The chip has been designed consisting of inflow and outflow ports, the distributor and collector with optimal geometry for achieving uniform flow distribution, the flow channel assembled with hundreds of single microchannels, and a pair of electrodes.

Microchannels with high-aspect-ratio of 5 and inter-channel distance of 50 μm prepared with silicon and PDMS have been fabricated by dry etching and soft lithography, carefully taking into account the process conditions during micromachining. To obtain the high-aspect-ratio flow channel in the silicon–glass chip, the DRIE has been applied following the anodic bonding.

The validity test including comparisons with theoretical computations shows that a higher magnitude of zeta potential of the silicon surface than that of the PDMS provides a higher streaming potential. In the same chip, the electric power density increases with increasing external resistance. The silicon–glass chip is shown to result in increasing the power density of above at least 3 times than in the case of the PDMS–glass one. Therefore, our performance evaluation can justify that the silicon-based microfluidic chip is more valid than the PDMS-based one as efficient electrokinetic streaming potential devices. Although the adoption of a multi-channel type microfluidic chip is a challenging issue in developing the well-established streaming potential devices, further studies are necessary to enhance the power density conducting more innovative stack system.

Nomenclature

A	cross-sectional area of microchannel/m^2
b_l	distance of longer base/m
b_s	distance of shorter base/m
e	elementary charge/C
$f_{(1)}$, $f_{(2)}$	coupled function (–)
H	height of a single channel/m
I	net electric current/A
I_C	conduction current/A
I_L	external current/A
I_S	streaming current, or convection current/A
kT	Boltzmann thermal energy/J
L	straight length of duct/m
l	length of a single channel/m
N	number of microchannels (–)
n	number concentration of ion species/m^{-3}
P_D	electric power density/A V m^{-3}
Q	flow rate/m^3 s^{-1}
R_T	total resistance of single microchannel/Ω
r_t	tapering rate of the distance (–)
S	inter-channel distance/m
v_z	axial fluid velocity/m s^{-1}
W	width of a single channel/m
Z	valence of ion species (–)

Greek letters

ε	dielectric constant, or permittivity of the medium/C^2 J^{-1} m^{-1}
ρ_e	net charge density/C m^{-3}
ϕ	flow-induced streaming potential/V
ϕ_L	streaming potential in the circuit with external resistance/V
ψ	electric potential/V

Acknowledgements

This work was supported by the Basic Research Fund (R01-2004-000-10944-0) from the Korea Science and Engineering Foundations (KOSEF). The authors wish to extend their sincere gratitude to the staff at the Micro-Nano Fabrication Center located in the KIST for valuable technical advice.

References

1 G. E. Karniadakis and A. Beskok, *Micro Flows: Fundamentals and Simulation*, Springer-Verlag, New York, 2002.
2 D. R. Reyes, D. Iossifidis, P.-A. Auroux and A. Manz, Micro Total Analysis Systems. 1. Introduction, Theory, and Technology, *Anal. Chem.*, 2002, **74**, 2623–2636.
3 L. C. Campbell, M. J. Wilkinson, A. Manz, P. Camilleri and C. J. Humphreys, Electrophoretic manipulation of single DNA molecules in nanofabricated capillaries, *Lab Chip*, 2004, **3**, 225–229.
4 N. A. Polson and M. A. Hayes, Electroosmotic flow control of fluids on a capillary electrophoresis microdevice using an applied external voltage, *Anal. Chem.*, 2000, **72**, 1088–1092.
5 H. A. Stone, A. D. Stroock and A. Ajdari, Engineering flows in small devices: microfluidics toward a lab-on-a-chip, *Annu. Rev. Fluid Mech.*, 2004, **36**, 381–411.
6 C. L. Rice and R. Whitehead, Electrokinetic flow in a narrow cylindrical capillary, *J. Phys. Chem.*, 1965, **69**, 4017–4024.
7 S. Levine, J. R. Marriott, G. Neale and N. Epstein, Theory of electrokinetic flow in fine cylindrical capillaries at high zeta-potentials, *J. Colloid Interface Sci.*, 1975, **52**, 136–149.
8 C. Werner, H. Körber, R. Zimmermann, S. Dukhin and H.-J. Jacobasch, Extended electrokinetic characterization of flat solid surfaces, *J. Colloid Interface Sci.*, 1998, **208**, 329–346.
9 M.-S. Chun, S.-Y. Lee and S.-M. Yang, Estimation of zeta potential by electrokinetic analysis of ionic fluid flows through a divergent microchannel, *J. Colloid Interface Sci.*, 2003, **266**, 120–126.
10 L. Ren, D. Li and W. Qu, Electro-viscous effects on liquid flow in microchannels, *J. Colloid Interface Sci.*, 2001, **233**, 12–22.
11 P. Vainshtein and C. Gutfinger, "On electroviscous effects in microchannels, *J. Micromech. Microeng.*, 2002, **12**, 252–256.
12 J. Yang, F. Lu, L. W. Kostiuk and D. Y. Kwok, Electrokinetic microchannel battery by means of electrokinetic and microfluidic phenomena, *J. Micromech. Microeng.*, 2003, **13**, 963–970.
13 W. Olthuis, B. Schippers, J. Eijkel and A. van den Berg, Energy from streaming current and potential, *Sens. Actuators, B*, 2005, **111–112**, 385–389.
14 M.-S. Chun, T. S. Lee and N. W. Choi, Microfluidic analysis of electrokinetic streaming potential induced by microflows of monovalent electrolyte solution, *J. Micromech. Microeng.*, 2005, **15**, 710–719.
15 Y. Jeong, S. Kim, K. Chun, J. Chang and D. S. Chung, Methodology for miniaturized CE and insulation on a silicon substrate, *Lab Chip*, 2001, **1**, 143–147.
16 W. M. Moreau, *Semiconductor Lithography: Principles, Practices and Materials*, Plenum Press, New York, 1988.
17 C.-H. Lin, G.-B. Lee, Y.-H. Lin and G.-L. Chang, A fast prototyping process for fabrication of microfluidic systems on soda-lime glass, *J. Micromech. Microeng.*, 2001, **11**, 726–732.

18 F. Ayazi and K. Najafi, High aspect-ratio polysilicon micromachining technology, *Sens. Actuators, A*, 2000, **87**, 46–51.
19 A. A. Ayón, X. Zhang and R. Khanna, Anisotropic silicon trenches 300–500 μm deep employing time multiplexed deep etching (TMDE), *Sens. Actuators, A*, 2001, **91**, 381–385.
20 M. Despont, H. Gross, F. Arrouy, C. Stebler and U. Staufer, Fabrication of a silicon-Pyrex-silicon stack by a.c. anodic bonding, *Sens. Actuators, A*, 1996, **55**, 219–224.
21 *Fundamentals of Microfabrication: The Science of Miniaturization*, ed. M. J. Madou, CRC Press, New York, 2nd edn, 2002.
22 T. R. Anthony, Dielectric isolation of silicon by anodic bonding, *J. Appl. Phys.*, 1985, **58**, 1240–1247.
23 L. Jiang, M. Wong and Y. Zohar, Forced convection boiling in a microchannel heat sink, *J. Microelectromech. Syst.*, 2001, **10**, 80–87.
24 Y. C. Chan, M. Carles, N. J. Sucher, M. Wong and Y. Zohar, Design and fabrication of an integrated microsystem for microcapillary electrophoresis, *J. Micromech. Microeng.*, 2003, **13**, 914–921.
25 B.-H. Jo, L. van Lerberghe, K. Motsegood and D. Beebe, Three-dimensional micro-channel fabrication in polydimethylsiloxane (PDMS) elastomer, *J. Microelectromech. Syst.*, 2000, **9**, 76–81.
26 J. C. McDonald and G. M. Whitesides, Poly(dimethylsiloxane) as a material for fabricating microfluidic devices, *Acc. Chem. Res.*, 2002, **35**, 491–499.
27 M.-S. Chun and S. Lee, Flow imaging of dilute colloidal suspension in PDMS-based microfluidic chip using fluorescence microscopy, *Colloids Surf., A*, 2005, **267**, 86–94.
28 R. F. Probstein, *Physicochemical Hydrodynamics: An Introduction*, Wiley, New York, 1994.